Supporting Information

High-Entropy 2D Carbide MXenes: $TiVNbMoC_3$ and $TiVCrMoC_3$

Srinivasa Kartik Nemani[1,2], Bowen Zhang[1,2,3], Brian C. Wyatt[1,2], Zachary D. Hood[4], Sukriti Manna[5, 6], Rasoul Khaledialidusti[7], Weichen Hong[1], Michael G. Sternberg[5], Subramanian K. R. S. Sankaranarayanan[5,6,*], Babak Anasori[1,2,*]

1. Department of Mechanical and Energy Engineering, Purdue School of Engineering and Technology, Indiana University-Purdue University Indianapolis, Indianapolis, Indiana, 46202, United States
2. Integrated Nanosystems Development Institute, Indiana University-Purdue University Indianapolis, Indianapolis, Indiana, 46202, United States
3. Permanent address: Henan Key Laboratory of Photovoltaic Materials, Henan University, Kaifeng 475004, P. R. China
4. Applied Materials Division, Argonne National Laboratory, Lemont, Illinois 60439, United States
5. Center for Nanoscale Materials, Argonne National Laboratory, Lemont, Illinois 60439, United States
6. Department of Mechanical and Industrial Engineering, University of Illinois, Chicago, Illinois 60607, United States
7. Department of Mechanical and Industrial Engineering, Norwegian University of Science and Technology (NTNU), 7491 Trondheim, Norway

* Address correspondence to: skrssank@uic.edu, banasori@iupui.edu

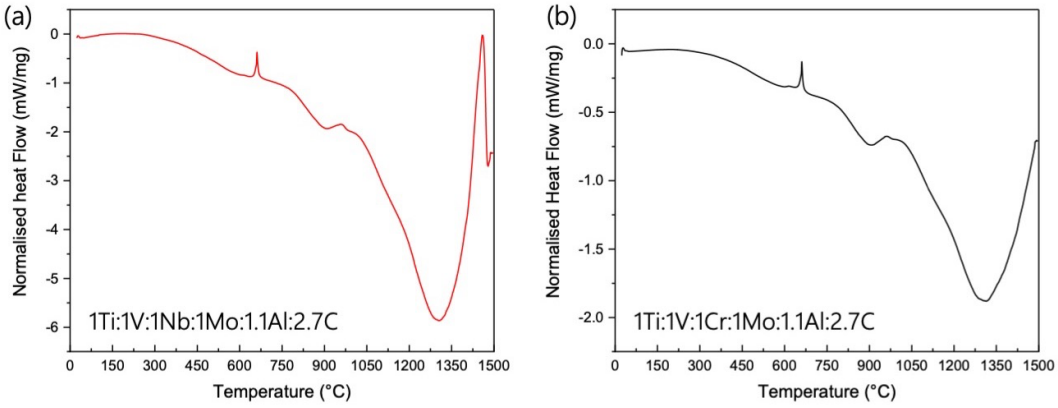

Figure S1: Differential scanning calorimetry results of a) Ti:V:Nb:Mo:1.1Al:2.7C, and b) Ti:V:Cr:Mo:1.1Al:2.7C powder mixtures under argon flow. Both powder mixtures have a peak between 653-664 ºC, which indicates the melting of Al and the start of reaction with the transition metals to form intermetallics. With the initiation of carbon diffusion, binary carbide can form, followed by phase stabilization and ternary carbide formation between 1250-1350 ºC, similar to previously studied MAX phases.[1, 2] At temperatures above 1450 ºC, high-entropy multi-principle element phases can form.

Table S1: EDS analysis of high-entropy MAX particles, multilayer (ML) MXene particles and delaminated (d-) MXene films. Four representative SEM images of the MAX particles that were used for EDS are shown for $TiVNbMoAlC_3$ and $TiVCrMoAlC_3$

	Ti	V	Cr	Nb	Mo	Al
EDS on particles						
$(Ti,V,Nb,Mo)_4AlC_3$	0.9 ± 0.2	1.1 ± 0.2	-	1.1 ± 0.2	0.9 ± 0.3	1.09 ± 0.2
ML-$(Ti,V,Nb,Mo)_4C_3T_x$	1.0 ± 0.1	1.0 ± 0.1	-	1.2 ± 0.4	0.8 ± 0.3	-
d-$(Ti,V,Nb,Mo)_4C_3T_x$	0.9 ± 0.2	1.0 ± 0.2	-	1.0 ± 0.2	0.9 ± 0.3	-
$(Ti,V,Cr,Mo)_4AlC_3$	1.0 ± 0.1	1.1 ± 0.1	1.0 ± 0.1	-	0.9 ± 0.1	1.16 ± 0.15
ML-$(Ti,V,Cr,Mo)_4C_3T_x$	1.1 ± 0.2	1.2 ± 0.1	0.8 ± 0.3	-	0.9 ± 0.1	
d-$(Ti,V,Cr,Mo)_4C_3T_x$	1.1 ± 0.2	1.1 ± 0.2	0.9 ± 0.2	-	1.0 ± 0.2	-

SEM images of $TiVNbMoAlC_3$

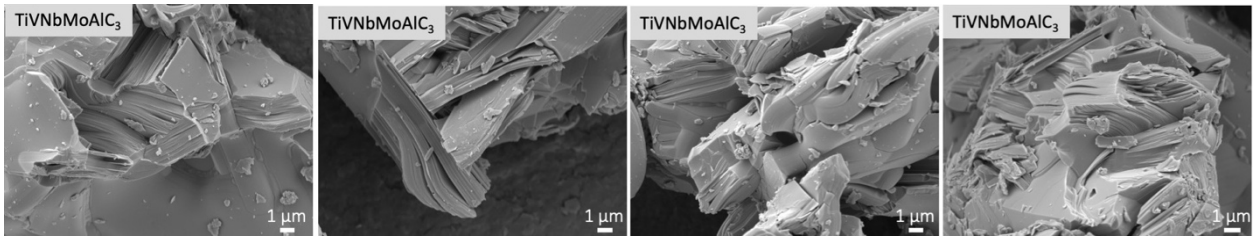

SEM images of $TiVCrMoAlC_3$

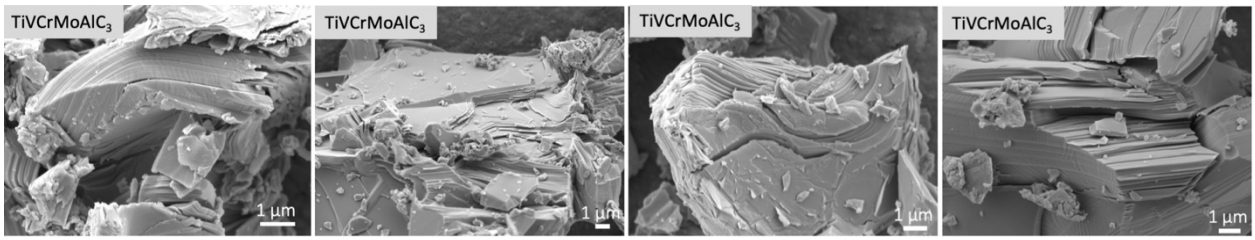

Reaction pathways from high-entropy MAX to MXene

$TiVNbMoAlC_3$ to $TiVNbMoC_3$

$TiVNbMoAlC_3 + 3HF = TiVNbMoC_3 + AlF_3 + 3/2H_2$

$TiVNbMoC_3 + 2H_2O = TiVNbMoC_3(OH)_2 + H_2$

$TiVNbMoC_3 + 2\ HF = TiVNbMoC_3F_2 + H_2$

$TiVCrMoAlC_3$ to $TiVCrMoC_3$

$TiVCrMoAlC_3 + 3HF = TiVCrMoC_3 + AlF_3 + 3/2H_2$

$TiVCrMoAlC_3 + 2H_2O = TiVCrMoC_3(OH)_2 + H_2$

$TiVCrMoAlC_3 + 2\ HF = TiVCrMoC_3F_2 + H_2$

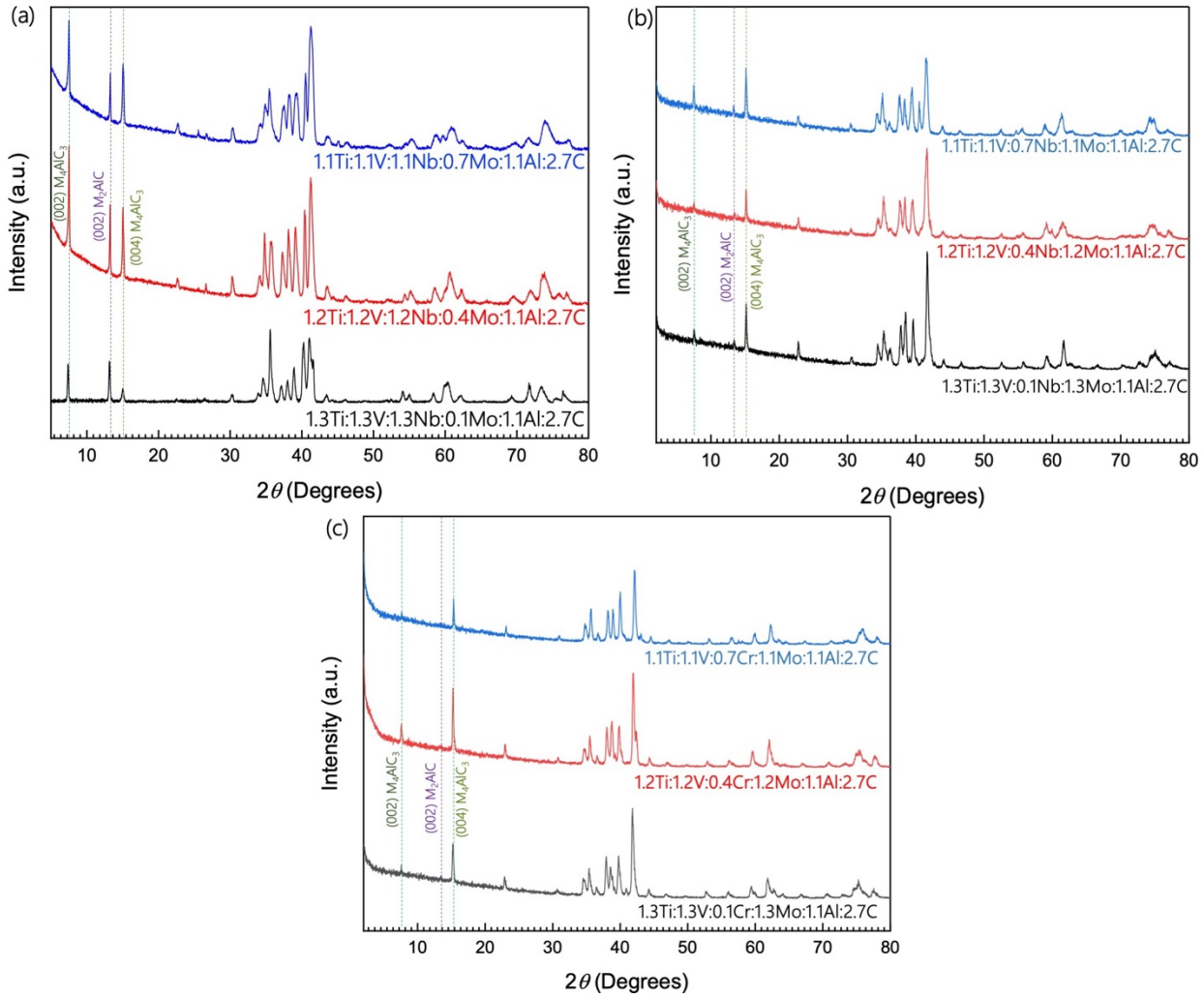

Figure S2: XRD spectra of multiphases formed by sintering different ratios of a) Ti:V:Nb:Mo with Mo variation, b) Ti:V:Nb:Mo with Nb variation, c) Ti:V:Cr:Mo with Cr variation and keeping 1.1Al:2.7C in all mixtures. Variation in the stoichiometric ratio of Mo in (a), Nb in (b), and Cr in (c) in these powder mixtures lead to the formation multiphases of M_2AlC along with M_4AlC_3, instead of a single-phase M_4AlC_3. This is evident from the presence of simultaneous (00*l*) peaks, (002) at ~ 7.5˚ for M_4AlC_3 and ~13.5˚ for M_2AlC.

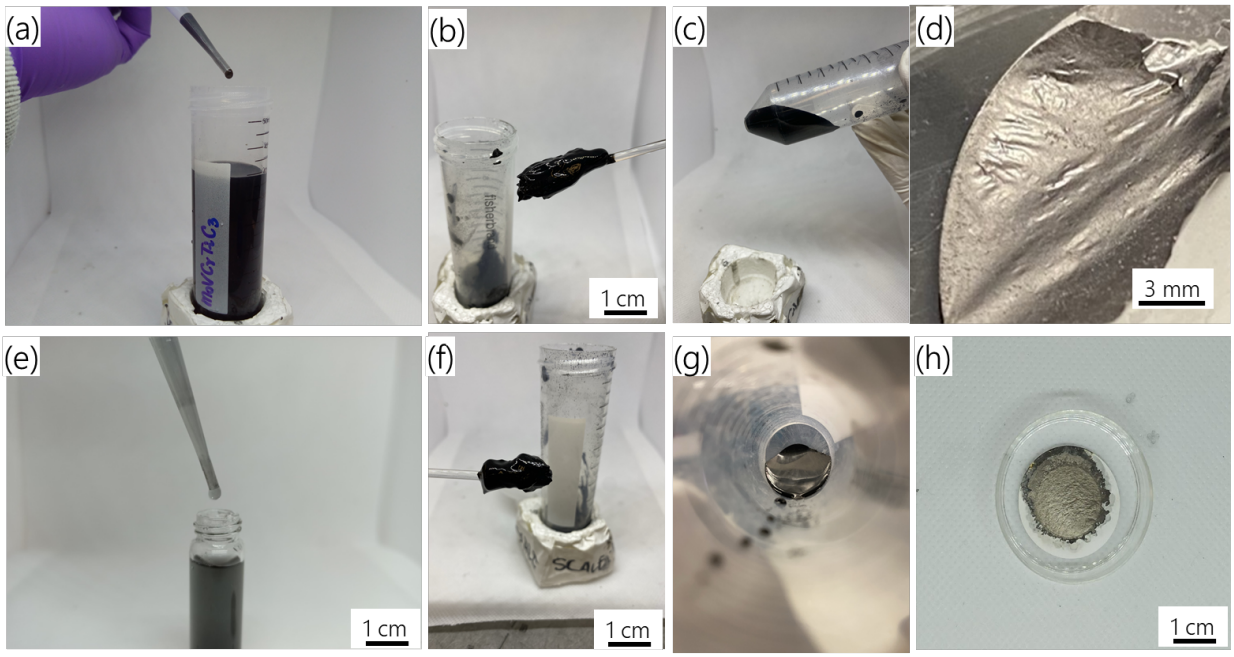

Figure S3: (a-d) $TiVCrMoC_3T_x$ at various stages of synthesis. (a) Single-flake MXene solution after delamination with TMAOH, (b,c) few-layer MXene clay post delamination, (d) MXene film doctor bladed on a 0.22-micron filter paper. (e-h) $TiVNbMoC_3T_x$ at various stages of synthesis. (e) Diluted single-flake MXene solution after delamination with TMAOH, (f,g) few-layer MXene clay post delamination, (h) MXene film filtered on a 0.22-micron filter.

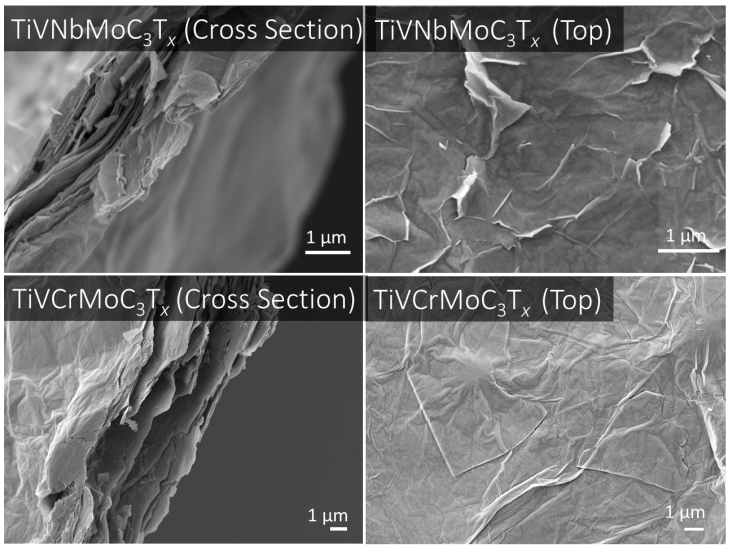

Figure S4: SEM images of $TiVNbMoC_3T_x$ and $TiVCrMoC_3T_x$ few-layered films. Cross sectional (left) and top view (right).

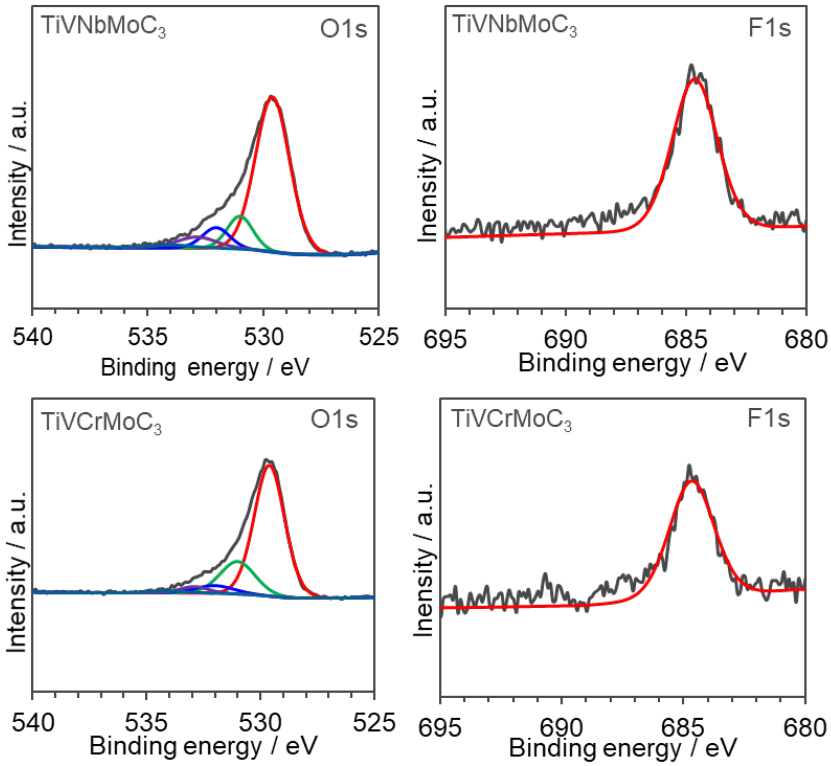

Figure S5: XPS spectra of $TiVNbMoC_3T_x$ and $TiVCrMoC_3T_x$ showing the surface functional groups –O and –F.

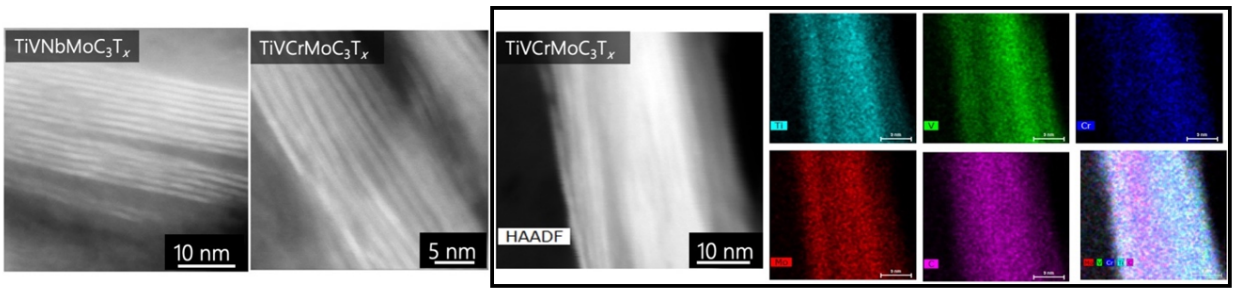

Figure S6: High-angle annular dark-field (HAADF) STEM images of delaminated (i) $TiVNbMoC_3T_x$ (left) and $TiVCrMoC_3T_x$ (right) MXenes, (ii) HAADF STEM image of $TiVCrMoC_3T_x$ with EDS data indicating atomic distribution of Ti, V, Cr, Mo, C atoms.

Table S2: XPS Deconvolution data with Binding Energy (BE), FWHM values for $TiVNbMoC_3T_x$. Deconvolution was performed using Thermo Avantage, a software package available through Thermo Scientific as well as references [3-5]

$TiVNbMoC_3T_x$				
Region	**BE (eV)**		**FWHM (eV)**	**Assigned to**
Ti 2p	454.8	461	1.3	Ti-C
	456.6	462.8	3.0	TiO_2
C 1s	282.2		1.0	C-Mo/Ti-T_x
	282.6		1.0	C-Ti/Mo-T_x
	284.8		1.7	C-C
	285.4		1.5	CH_x
	286.2		2.0	C-O
	287.5		2.0	COO
O 1s	530		1.5	MoO_x/TiO_2/C-Mo-O(I)
	530.9		1.1	C-Mo-O(II)x and/or OR
	531.9		1.2	C-Mo-$(OH)_x$ and/or OR
	533		1.4	H_2Oads (IV) and/or OR
Mo 3d	228	231.1	1.1	Mo metal
	229.3	232.5	1.1	C-Mo-T_x
	230.5	233.9	1.3	Mo^{+5}
	232	235.1	1.4	Mo^{+6}
Nb 3d	203.1	205.9	0.7	Nb
	203.5	206.3	0.8	Nb
	203.8	206.6	0.9	Nb (I, II, or IV)
	204.1	206.9	0.8	NbO
	205.2	208.0	0.9	$Nb(^{3+})$-O
	206.7	209.5	0.6	$Nb(^{4+})$-O
	207.4	210.2	0.8	Nb_2O_5
V 2p	513.6	521	1.5	V^{2+}
	516.4	523.8	2.0	V^{4+}
	517.1	524.5	1.5	V_2O_3

Region	BE (eV)	FWHM (eV)	Assigned to
O1s	529.6	1.8	TiO_2, MO_x
	531.0	1.4	C-M-O_x (I)
	532.0	1.5	C-M-OH_x (II)
	532.9	2.0	Al_2O_3
	534.0	2.0	H_2O_{ads} (IV)
F1s	684.6	2.3	M-F

Table S3: XPS Deconvolution data with Binding Energy (BE), FWHM values for $TiVCrMoC_3T_x$. Deconvolution was performed using Thermo Avantage, a software package available through Thermo Scientific as well as references [3-5]

$TiVCrMoC_3T_x$				
Region	**BE (eV)**		**FWHM (eV)**	**Assigned to**
Ti 2p	454.8	461	1.5	Ti-C
	456.6	462.8	3.0	TiO_2
C 1s	282.3		1.0	C-Mo/Ti-T_x
	282.7		1.1	C-Ti/Mo-T_x
	284.8		1.7	C-C
	285.5		1.5	CH_x
	286.3		2.0	C-O
	287.6		2.0	COO
O 1s	530		1.6	MoOx/TiO_2/C-Mo-O(I)
	530.9		1.2	C-Mo-$O(II)_x$ and/or OR
	531.9		1.2	C-Mo-$(OH)_x$ and/or OR
	533		1.4	H_2O_{ads} (IV) and/or OR
Mo3d	228	231.1	1.1	Mo metal
	229.3	232.5	1.2	C-Mo-T_x
	230.5	233.9	1.3	Mo^{+5}
	232	235.1	1.4	Mo^{+6}
Cr2p	574.8	584.1	2.0	Cr-C
	576.4	585.7	2.8	Cr-T_x
V 2p	513.6	521	1.5	V^{2+}
	515.4	522.8	2.0	V^{4+}
	517.1	524.5	1.5	V_2O_3

$TiVCrMoC_3$

Region	BE (eV)	FWHM (eV)	Assigned to
O1s	529.6	1.6	TiO_2, MO_x
	531.0	1.9	C-M-O_x (I)
	532.0	2.0	C-M-OH_x (II)
	532.9	1.5	Al_2O_3
	534.0	2.0	H_2O_{ads} (IV)
F1s	684.6	2.2	M-F

Table S4: List of MAX phases. a, b, and c are the lattice parameters. ΔH_{cp} indicates the formation enthalpy of MAX phases over competing phases at 0 Kelvin

MAX Phases	a (Å)	b (Å)	c (Å)	Most competing phases	ΔH_{cp} (eV/atom)	Electron Concentration (electron/Å^3)
(TiVCrMo)AlC_3	2.985	2.985	23.066	Ti_3AlC_2, V_3AlC_2, Cr_3C_2, Mo_3Al, C	-0.011	0.405
(TiVNbMo)AlC_3	3.055	3.054	23.601	Ti_3AlC_2, V_3AlC_2, Nb_3AlC_2, MoC	0.033	0.367
$(Ti_{1.33}V_{1.33}Nb_{1.33})AlC_3$	3.044	3.050	23.557	Ti_3AlC_2, V_3AlC_2, Nb_3AlC_2, C	0.014	0.356

Probable reaction paths for formation of high-entropy MAX phases for Table S4

(TiVCrMo)AlC_3 ⇌ 1/3 Ti_3AlC_2 + 1/3 V_3AlC_2 + 1/3 Cr_3C_2 + 1/3 Mo_3Al + C

(TiVNbMo)AlC_3 ⇌ 1/3 Ti_3AlC_2 + 1/3 V_3AlC_2 + 1/3 Nb_3AlC_2 + MoC

$(Ti_{1.33}V_{1.33}Nb_{1.33})AlC_3$ ⇌ 1/3 Ti_3AlC_2 + 1/3 V_3AlC_2 + 1/3 Nb_3AlC_2 + C

Table S5: Bader Charges of the transition metals in $TiVCrMoAlC_3$ and $TiVCrMoAlC_3$

Composition	Ti	V	Cr/Nb	Mo
$TiVCrMoAlC_3$	1.307	1.121	0.893	0.759
$TiVNbMoAlC_3$	1.314	1.126	1.308	0.778

Table S5 results show that Ti elements gain more charge in $TiVNbMoAlC_3$ than $TiVCrMoAlC_3$, while the charge of V and Mo elements are identical in both compositions. Also, more charges are

transferred to the Nb element in $TiVNbMoAlC_3$ composition in comparison to the Cr element in $TiVNbMoAlC_3$ because the Nb and Cr elements need three and two electrons to fill their valence shell, respectively.

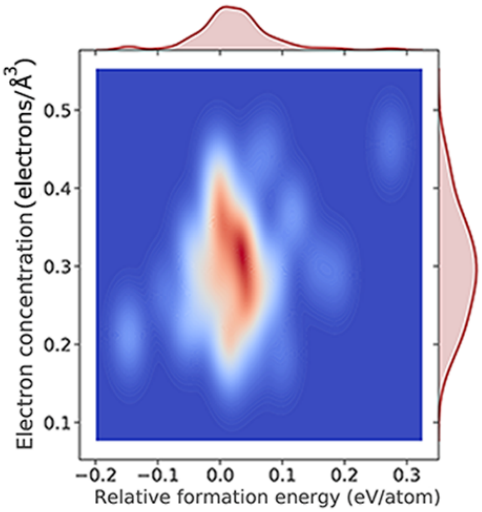

Figure S7. Calculated electron concentration of the already synthesized MAX phases with reference to their relative formation energy.

No specific value for ΔH_{cp} can be directly applied as a constraint for the thermodynamic stabilities of the MAX candidates. This is because the formation of many metastable materials is possible by controlling the temperature, pressure, and synthesis method. However, as stated, a lower value of ΔH indicates a higher probability of the MAX phase formation. The calculated ΔH_{cp} values (eV/atom) at 0 Kelvin for the MAX phases confirm that MAX phases of Sc_2AlC, Ti_2AlC, Ti_3AlC_2, and Ti_4AlC_3 with the ΔH_{cp} values of 0.10, 0.039, 0.039 and 0.038 eV/atom respectively, have already been synthesized.[6] Both an inadequate number of valence electrons occupying bonding states and an abundance of valence electrons occupying antibonding states reduce the probability of the successful synthesis of the MAX candidates [7].

We calculated the electron concentration for the MAX phases that have already been synthesized with reference to their relative formation energies (**Figure S7**). As shown, the synthesizability of MAX candidates is higher in those candidates with an electron concentration close to 0.3 (electrons/atom); however, no MAX phases have been formed with the electron concentration below 0.2 and above 0.43 (electrons/atom).

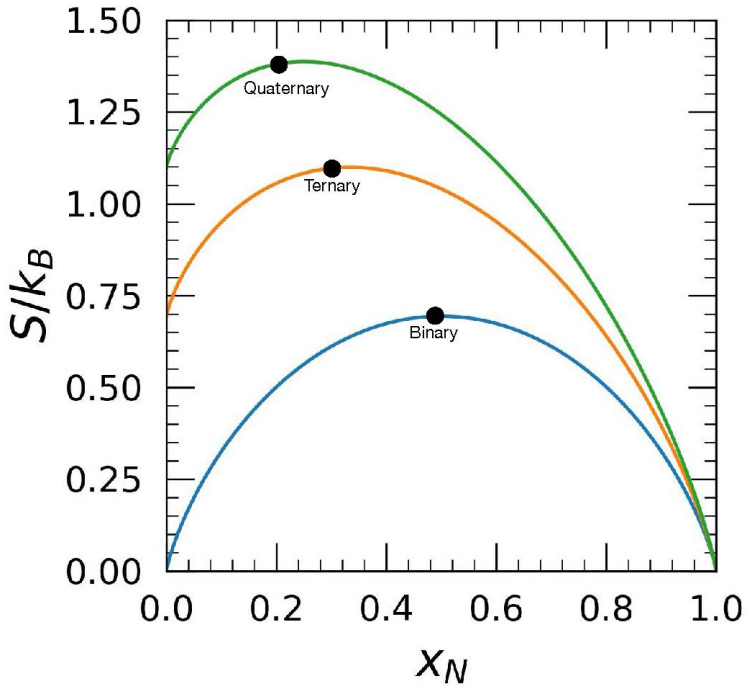

Figure S8. Calculated configurational entropy in a two, three, and four-component solid solutions as a function of mol% of the N_{th} component.[8]

References

1. Bandyopadhyay, D.; Sharma, R.; Chakraborti, N., The Ti-Al-C System (Titanium-Aluminum-Carbon). *Journal of phase equilibria* **2000,** *21* (2), 195.
2. Shuck, C. E.; Han, M.; Maleski, K.; Hantanasirisakul, K.; Kim, S. J.; Choi, J.; Reil, W. E.; Gogotsi, Y., Effect of Ti_3AlC_2 MAX Phase on Structure and Properties of Resultant $Ti_3C_2T_x$ MXene. *ACS Applied Nano Materials* **2019,** *2* (6), 3368-3376.
3. Halim, J.; Cook, K. M.; Eklund, P.; Rosen, J.; Barsoum, M. W., XPS of Cold Pressed Multilayered and Freestanding Delaminated 2D Thin Films of $Mo_2TiC_2T_z$ and $Mo_2Ti_2C_3T_z$ (MXenes). *Applied Surface Science* **2019,** *494*, 1138-1147.
4. Halim, J.; Cook, K. M.; Naguib, M.; Eklund, P.; Gogotsi, Y.; Rosen, J.; Barsoum, M. W., X-Ray Photoelectron Spectroscopy of Select Multi-Layered Transition Metal Carbides (MXenes). *Applied Surface Science* **2016,** *362*, 406-417.
5. Chastain, J.; King Jr, R. C., Handbook of X-Ray Photoelectron Spectroscopy. *Perkin-Elmer Corporation* **1992,** *40*, 221.
6. Khaledialidusti, R.; Khazaei, M.; Khazaei, S.; Ohno, K., High-Throughput Computational Discovery of Ternary-Layered MAX Phases and Prediction of Their Exfoliation for Formation of 2D MXenes. *Nanoscale* **2021**, 13, 7294-7307.
7. Gelatt Jr, C.; Williams, A.; Moruzzi, V., Theory of Bonding of Transition Metals to Nontransition Metals. *Physical Review B* **1983,** *27* (4), 2005.
8. Rost, C. M.; Sachet, E.; Borman, T.; Moballegh, A.; Dickey, E. C.; Hou, D.; Jones, J. L.; Curtarolo, S.; Maria, J.-P., Entropy-Stabilized Oxides. *Nature Communications* **2015,** *6* (1), 1-8.